

MIUSCAT: extended MILES spectral coverage. I. Stellar populations synthesis models.

A. Vazdekis^{1,2*}, E. Ricciardelli³, A.J. Cenarro⁴, J. G. Rivero-González⁵,
 L. A. Díaz-García⁴, J. Falcón-Barroso^{1,2}

¹*Instituto de Astrofísica de Canarias, Vía Lactea s/n, E-38200 La Laguna, Tenerife, Spain*

²*Departamento de Astrofísica, Universidad de La Laguna, E-38205, Tenerife, Spain*

³*Departament d'Astronomia i Astrofísica, Universitat de Valencia, c/ Dr. Moliner 50, E-46100 - Burjassot, Valencia, Spain*

⁴*Centro de Estudios de Física del Cosmos de Aragón, Plaza de San Juan 1, Planta 2, E-44001, Teruel, Spain*

⁵*Universitätssternwarte München, Scheinerstr. 1, 81679 München, Germany*

Accepted ... Received ...; in original form ...

ABSTRACT

We extend the spectral range of our stellar population synthesis models based on the MILES and CaT empirical stellar spectral libraries. For this purpose we combine these two libraries with the Indo-U.S. to construct composite stellar spectra to feed our models. The spectral energy distributions (SEDs) computed with these models and the originally published models are combined to construct composite SEDs for single-age, single-metallicity stellar populations (SSPs) covering the range $\lambda\lambda$ 3465 – 9469 Å at moderately high, and uniform, resolution (FWHM=2.51Å). The colours derived from these SSP SEDs provide good fits to Galactic globular cluster data. We find that the colours involving redder filters are very sensitive to the IMF, as well as a number of features and molecular bands throughout the spectra. To illustrate the potential use of these models we focus on the NaI doublet at 8200 Å and with the aid of the newly synthesized SSP model SEDs we define a new IMF-sensitive index that is based on this feature, which overcomes various limitations from previous index definitions for low velocity dispersion stellar systems. We propose an index-index diagram based on this feature and the neighboring CaII triplet at 8600 Å, to constrain the IMF if the age and [Na/Fe] abundance are known. Finally we also show a survey-oriented spectrophotometric application which evidences the accurate flux calibration of these models for carrying out reliable spectral fitting techniques. These models are available through our user-friendly website.

Key words: galaxies: abundances – galaxies: elliptical and lenticular,cD – galaxies: evolution – galaxies: stellar content – globular clusters: general – stars: fundamental parameters

1 INTRODUCTION

A quantitative study of the stellar content of galaxies and star clusters requires the use of the so called stellar population synthesis models. The method consists in comparing observables like colours, line-strength indices or full spectral energy distributions (SEDs) to the predictions of these models (e.g., Tinsley 1980). Furthermore these models are widely employed in many other type of studies such as, e.g., to provide the necessary templates for kinematic or redshift measurement or to determine galaxy stellar masses with the aid of the mass-to-light ratios (M/L). Most recent models

employ at least three main ingredients, which determine the quality of the predictions: a prescription for the initial mass function (IMF), a set of stellar evolutionary isochrones and stellar spectral libraries. Galaxy observables are predicted by adding the contributions of all possible stars, in proportions prescribed by stellar evolution models. The required SEDs, colours or absorption line-strengths of all these stars are obtained from the stellar libraries.

Colours, absorption line-strengths and other observables from these models have been widely used in the literature for interpreting the integrated light of stellar clusters and galaxies. In the recent years, it has become common practice to use model SEDs, mainly for single-burst stellar populations (SSPs), at moderately high spectral resolution. These models provide new means for lifting the

* E-mail: vazdekis@iac.es

main degeneracies hampering stellar populations studies, such as the one between the age and the metallicity (e.g., Worthey 1994). For example these SEDs have allowed us to define new indices with enhanced abilities to disentangle the age from the metallicity (e.g., Vazdekis & Arimoto 1999; Cervantes & Vazdekis 2009), or even the IMF (e.g., Schiavon et al. 2000; Vazdekis et al. 2003). In recent years it is becoming increasingly popular to use these model SEDs to derive relevant stellar population parameters, including the Star Formation History (SFH), by means of full spectrum-fitting approach (e.g., Cid Fernandes et al. 2005; Koleva et al. 2009; Tojeiro et al. 2011), which represents an alternative to the more standard approach of fitting a selected number of line-strength indices (see, e.g., Trager et al. 1998, and references therein). Furthermore these model SEDs have been used in a variety of applications. For example, these SSP SEDs have been shown to improve the analysis of galaxy kinematics for both absorption and emission lines (e.g., Falc3n-Barroso et al. 2003; Sarzi et al. 2006).

There are models that are fed with theoretical stellar atmospheres (e.g., Schiavon et al. 2000; Gonz1lez-Delgado et al. 2005; Coelho et al. 2007), whereas other models employ empirical libraries, mostly in the visible (e.g., Vazdekis 1999; Bruzual & Charlot 2003; Le Borgne et al. 2004; Conroy & Gunn 2010; Vazdekis et al. 2010; Maraston & Str3mb1ck 2011; Conroy & van Dokkum 2011), but also in other spectral ranges (e.g., Vazdekis et al. 2003; Conroy & van Dokkum 2011; Maraston & Str3mb1ck 2011). Models based on empirical libraries are free from the uncertainties in the underlying model atmospheric calculations and tend to provide good fits to both, absorption line-strengths and spectra (e.g. Vazdekis et al. 2010; Maraston & Str3mb1ck 2011 and photometric data (e.g., Maraston et al. 2009; Peacock et al. 2011). Unlike the models based on theoretical libraries, these models are generally restricted in their SSP parameter coverage, as most of the stars come from the solar neighbourhood, with e.g. a limited metallicity and elemental abundance ratio coverage. The quality of the resulting model SEDs relies to a great extent on the atmospheric parameters (temperature, gravity and metallicity) coverage of the library.

We published model SEDs in the near-IR at 1.5 Å (FWHM) resolution (Vazdekis et al. 2003) and in the optical range (Vazdekis et al. 2010) at FWHM=2.51 Å (Falc3n-Barroso et al. 2011), which employ the CaT and MILES empirical stellar spectral libraries of Cenarro et al. (2001) and S1nchez-Bl1zquez et al. (2006), respectively. These libraries show improved coverage of the stellar parameters and good flux-calibration quality among other characteristics. Unfortunately there is a spectral gap around 8000 Å, of about 900 Å, which is not covered between these two model SED predictions. This gap prevents us to derive a variety of widely employed colours, from *U* to *I* broad band filters, and to exploit potentially interesting absorption features in that spectral region, such as the NaI at 8200 Å, which has been shown to be useful for constraining the dwarf/giant ratios in galaxies (e.g. Faber & French 1980).

This is the first paper of a series where we present the extended spectral coverage of the SEDs predicted by our stellar population synthesis models. For this purpose we make use of the Indo-U.S. stellar spectral library

(Valdes et al. 2004) to fill-in this gap and to extend blueward and redward the spectral coverage of our model SEDs. These SEDs constitute an extension of our "base models", as we combine scaled-solar isochrones with empirical stellar spectral libraries, which follow the chemical evolution pattern of the solar neighbourhood. The models rely as much as possible on empirical ingredients, not just on the stellar spectra, but also on extensive photometric libraries, which are used to determine the transformations from the theoretical parameters of the isochrones to observational quantities. Our predicted SEDs are therefore self-consistent, and scaled-solar for solar metallicity. In the low metallicity regime, however, our models combine scaled-solar isochrones with stellar spectra that do not show this abundance ratio pattern (e.g., Edvardsson et al. 1993; Schiavon 2007). An extensive comparison of the predicted photometric properties with data of globular clusters of the MW and M 31 and early-type galaxies from the SDSS is shown in a second paper (Ricciardelli et al. 2012; hereafter Paper II).

The paper is organized as follows. In Section 2 we show the main ingredients of our models, including the composite stellar spectral library that we constructed to feed these models. In Section 3 we describe the reliability and quality of the resulting models and the behaviour of the MIUSCAT SSP SEDs and colours derived from these spectra. Section 4 illustrates with various examples the potential use of these models. In Section 5 we describe the web-based user-friendly facilities to download and handle these model SEDs. Finally in Section 6 we summarize our results.

2 MODELS

The MIUSCAT SSP SEDS presented here represent an extension of the models published in Vazdekis et al. (2003) and Vazdekis et al. (2010) to cover the whole spectral range $\lambda\lambda$ 3465 - 9469 Å. We provide here a brief summary of the main ingredients employed by these models and focus on the new addition that allows us to achieve such spectral range extension, i.e. the MIUSCAT stellar spectral library.

2.1 Main ingredients

We employ the solar-scaled theoretical isochrones of Girardi et al. (2000), which cover a wide range of ages, well sparsed from 0.063 to 17.8 Gyr, and six metallicity bins ($Z = 0.0004, 0.001, 0.004, 0.008, 0.019$ and 0.03), where 0.019 represents the solar value. The isochrones include the latest stages of the stellar evolution, including a simple synthetic prescription for incorporating the thermally pulsing AGB regime to the point of complete envelope ejection. The range of initial stellar masses extends from 0.15 to $7M_{\odot}$. The input physics of these models was updated with respect to Bertelli et al. (1994) with an improved version of the equation of state, the opacities of Alexander & Ferguson (1994) and a milder convective overshoot scheme. A helium fraction was adopted according to the relation: $Y \approx 0.23 + 2.25Z$.

We use the theoretical parameters of the isochrones ($T_{\text{eff}}, \log g, [Z/H]$) to obtain stellar fluxes on the basis of empirical relations between colours and stellar parameters (temperature, metallicity and gravity), instead of using theoretical stellar atmospheres. We mostly use the

metallicity-dependent empirical relations of Alonso et al. (1996, 1999); respectively, for dwarfs and giants. Each of these libraries are composed of ~ 500 stars and the obtained temperature scales are based on the IR-Flux method, i.e. only marginally dependent on model atmospheres. We use the empirical compilation of Lejeune et al. (1997); Lejeune, Cuisinier, & Buser (1998) (and references therein) for the coolest dwarfs ($T_{\text{eff}} \leq 4000 \text{ K}$) and giants ($T_{\text{eff}} \leq 3500 \text{ K}$) for solar metallicity, and also for stars with temperatures above $\sim 8000 \text{ K}$. For these low temperatures we use a semi-empirical approach to other metallicities on the basis of these relations and the model atmospheres of Bessell et al. (1989, 1991) and the library of Fluks et al. (1994). We also employ the metal-dependent bolometric corrections given by Alonso et al. (1995, 1999) for dwarfs and giants, respectively. We adopt $BC_{\odot} = -0.12$ and a bolometric magnitude of 4.70 for the Sun.

Several IMFs are considered: the two power-law IMFs described in Vazdekis et al. (1996) (i.e. unimodal and bimodal), the two characterized by its slope μ as a free parameter, and the multi-part power-law IMFs of Kroupa (2001) (i.e. universal and revised). The Salpeter (1955) IMF is obtained by adopting the unimodal case with slope $\mu = 1.3$. An extensive description of these definitions is given in V03 (Appendix A). We set the lower and upper mass-cutoff of the IMF to 0.1 and $100 M_{\odot}$, respectively.

2.2 MIUSCAT stellar spectral library

To extend the spectral coverage of our MILES-based models (Vazdekis et al. 2010) we employ three empirical stellar libraries at moderately-high spectral resolution: MILES (Sánchez-Blázquez et al. 2006) and the near-IR CaT library of Cenarro et al. (2001), both with very good relative flux-calibration, and the Indo-U.S.¹ (Valdes et al. 2004), which covers a significantly wider spectral range. This library allows us to fill-in the gap left between the MILES and CaT libraries and to extend the wavelength coverage slightly blueward of MILES and redward of the CaT library.

MILES includes 985 stars covering the range $3525\text{--}7500 \text{ \AA}$ with a spectral resolution of 2.5 \AA (FWHM), as recently shown in Falcón-Barroso et al. (2011). The CaT library (Cenarro et al. 2001) consists of 706 stars in the range $8350\text{--}9020 \text{ \AA}$ at resolution 1.5 \AA . The INDO-U.S. library includes ~ 1200 stars with spectra that typically cover from 3465 to 9469 \AA . In Falcón-Barroso et al. (2011) we also have recently shown that the spectral resolution of this library is slightly larger (FWHM= 1.36 \AA) than the approximate value provided in the original Indo-U.S. paper (FWHM $\sim 1.2 \text{ \AA}$).

The atmospheric parameters of all the Indo-U.S. stars in common with MILES and/or CaT libraries have been compared in order to calculate the necessary transformations for obtaining an homogenized set of stellar parameters with MILES. From this comparison we obtained

$$\text{Teff}_M = 1.02\text{Teff}_{IU} - 108.31 \quad (1)$$

$$\log g_M = 1.0467 \log g_{IU} - 0.1077 \quad (2)$$

$$[\text{Fe}/\text{H}]_M = [\text{Fe}/\text{H}]_{IU} - 0.02 \quad (3)$$

As it can be seen, a linear correction was required to bring the published Indo-U.S. temperatures and gravities onto the MILES/CaT system, whereas the metallicities were matched by applying a small offset.

We selected the Indo-U.S. stars whose spectra cover the desired wavelength range without gaps. We ended up with 574 stars, from which 142 have been removed due to the presence of strong telluric absorption residuals in their spectra. The final catalog is composed of 432 stars. Finally we flagged 76 of these stars for showing moderate telluric residuals.

In order to obtain a constant resolution and dispersion value within the desired spectral range (3465 to 9469 \AA) for the composite MIUSCAT spectra, we first convolved the CaT and Indo-U.S. spectra with the required gaussian kernels to match the lower resolution of MILES (FWHM= 2.5 \AA). The next step consisted in resampling the smoothed spectra to match the dispersion of MILES (0.9 \AA).

Unlike the MILES and CaT libraries the flux-calibration of the Indo-U.S. spectra is not very good as a narrow slit was employed during the observations to achieve a moderately high spectral resolution (see Valdes et al. 2004 for details).

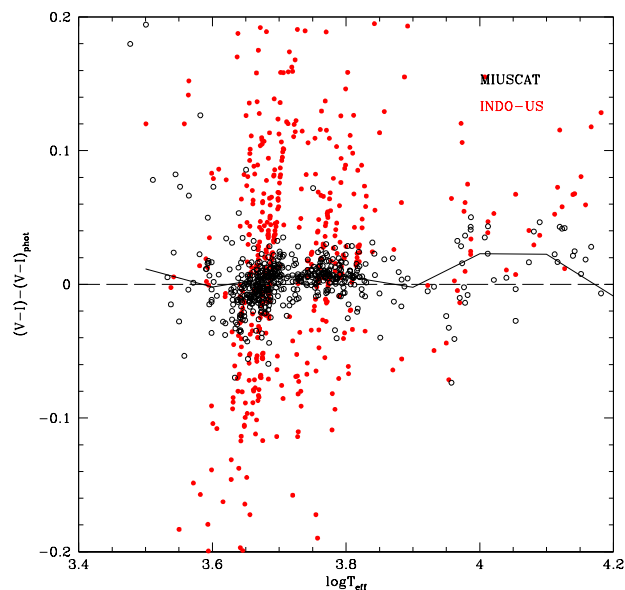
We use the Indo-U.S. spectra to fill-in the gap left between MILES and CaT spectral ranges, and also to extend toward the blue and red the wavelength coverage of MILES and CaT libraries, respectively. For each of the selected Indo-U.S. stars we use the MILES and/or CaT spectra, when available, and then plug the relevant Indo-U.S. spectral ranges to construct the composite MIUSCAT stellar spectrum. We find 208 stars in common to these three libraries. There are 150 Indo-U.S. stars in common with MILES and 114 in common with CaT. If a star is not present in either MILES or CaT, or even in these two libraries, we use the interpolators described in Vazdekis et al. (2010) and Vazdekis et al. (2003) to synthesize the corresponding MILES and CaT spectra, respectively.

To join the stellar spectra we first calibrate the Indo-U.S. spectrum in the region of the gap present between MILES and CaT. The relative flux scale of the MILES and CaT spectra is set by forcing the spectra to have the $V - I$ color corresponding to its stellar parameters, following the method described in V03 (Section 3.2.1). The $V - I$ color is derived from the photometric relations described in Section 2.1. Note that this method ensures a consistent approach throughout the various steps of the model computations. The Indo-U.S. spectrum in the gap is forced to overlap the MILES and CaT spectra at their red and blue edges, respectively. This is performed by approximating the continuum shape of the original and re-scaled Indo-U.S. spectra in the gap with a straight line joining the points at $\lambda\lambda 7360\text{--}7385 \text{ \AA}$ and $\lambda\lambda 8390\text{--}8415 \text{ \AA}$ (see Table 1). The Indo-U.S. spectrum is then scaled according to the ratio between the flux values on these two straight lines on each of the pixels. In the Indo-U.S. edges, i.e. bluewards MILES and redwards CaT, the INDO-U.S. spectrum is simply re-scaled to match the MILES and CaT continua. We scale the relevant Indo-U.S. spectral range by matching the flux of the MILES and CaT spectra in well selected narrow bands located at nearly the edges of spectral ranges of these libraries. These overlapping bands are chosen to be sufficiently wide to achieve the statistics. However these bands are sufficiently narrow to avoid prominent absorption features and to enable to use most of the MILES and CaT spectral ranges. The limiting

¹ <http://www.noao.edu/cfib/>

Table 1. Adopted merging wavelength ranges for matching the stellar spectra of the Indo-U.S., MILES and CaT libraries.

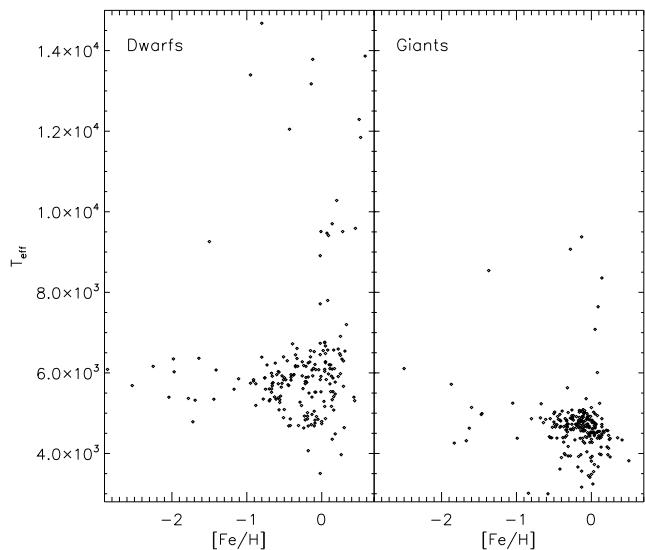
Libraries	Overlap wavelength range (\AA)
Indo-U.S.,MILES	3540 – 3564
MILES,Indo-U.S	7360 – 7385
Indo-U.S,CaT	8390 – 8415
CaT,Indo-U.S	8926 – 8950

**Figure 1.** We plot against $\log T_{\text{eff}}$ the residuals obtained by comparing the synthetic $(V - I)$ colour to the expected colour value $((V - I)_{\text{phot}})$ for the MIUSCAT stars. The latter values are obtained by applying the empirical photometric relations described in Section 2.1 according to the stellar parameters. The synthetic colours are obtained by convolving the resulting MIUSCAT (black open symbols) and the original Indo-U.S. (red solid symbols) stellar spectra with the filter responses (Johnson-Cousin system). Note the large dispersion obtained with the original Indo-U.S. spectra due to the limited flux-calibration quality (see the text for details). The solid black line represents the median of the MIUSCAT residuals for equally spaced logarithmic temperature interval.

wavelengths of the selected overlapping wavelength regions are listed in Table 1.

Finally as the limiting wavelengths of the spectral range covered by each stellar spectrum of the Indo-U.S. library differs slightly from each other we consider a common range for all the stars ($\lambda\lambda$ 3464.9 – 9468.8 \AA).

In Fig. 1 we show the residuals for the synthetic $V - I$ colours of both, the resulting MIUSCAT and the original Indo-U.S. spectra, compared to the expected colour values as a function of temperature. The latter are obtained by applying the empirical photometric relations described in Section 2.1, which are based on extensive photometric libraries, according to the stellar parameters. The synthetic colours are obtained by convolving the stellar spectra with the filter responses (Johnson-Cousin system). As expected the original Indo-U.S. spectra show large residuals due to the

**Figure 2.** The fundamental parameter coverage of the MIUSCAT stars is shown for dwarfs (left panel) and giants (right panel).

limited flux-calibration quality. The composite MIUSCAT stellar spectra show good agreement with the expected photometric colours. Indeed for the vast majority of the stars we obtain residuals smaller than the photometric zero-point (i.e. ~ 0.02 mag).

2.2.1 Stellar atmospheric parameter coverage

Figure 2 shows the parameter coverage of the MIUSCAT stars for dwarfs and giants (separated at $\log g = 3$). The parameters of the MIUSCAT stars plotted here are on the MILES system, which is the result of an extensive compilation from the literature, homogenized by taking as a reference the stars in common with Soubiran et al. (1998) (see Cenarro et al. 2007). Fig. 2 shows that, at solar metallicity, all types of stars are well represented. For metallicities lower than $[\text{Fe}/\text{H}] \sim -0.8$, however, the coverage is rather poor and therefore no reliable models can be computed. For the metallicity range between solar and $[\text{Fe}/\text{H}] \sim -0.8$ the coverage of both dwarfs and giants is good, with the notably exception of dwarfs with temperatures above ~ 7000 K. As these stars may represent the hotter Main Sequence, including the Turn Off, the resulting model predictions will be of lower quality in comparison to those for the older ages. Finally the coverage of metal-rich dwarf and giant stars allows us to safely compute SSP SEDs for $[\text{Z}/\text{H}] \sim 0.2$, including for the young and intermediate age regimes. A quantitative analysis of the quality of the models based on the atmospheric parameter coverage of MIUSCAT is provided in Section 2.3.

2.2.2 U magnitude

Since the bluest wavelength of the MIUSCAT spectra is 3464.9 \AA , we cannot accurately measure the flux in the Johnson U band, as this filter starts at ≈ 3050 \AA (Buser & Kurucz

1978). A similar situation applies to the SDSS u filter. As these filters are commonly used in the literature and the MIUSCAT spectral range provides most, but not all, the flux in these bands we have estimated the required corrections to be able to predict these quantities from the resulting MIUSCAT SSP model SEDs. To estimate the missing flux bluewards 3464.9 Å we employ the Pickles (1998) library of stars, which covers the spectral range $\lambda\lambda$ 1150-25000 Å at low resolution. Note that this library is mainly composed by solar metallicity stars. We estimate the missing fluxes by convolving the Pickles spectra with the filter responses of these bands to obtain both the total flux and the flux in the wavelength range covered by MIUSCAT, i.e. redwards 3464.9 Å.

The correction factors, given by the missing flux divided by the total flux, for the Johnson U filter, f_U , are shown in Fig. 3 for the different spectral types by adopting the two, the limiting wavelengths of MILES (upper panel) and MIUSCAT (lower panel). Despite the fact that MIUSCAT only extends to the blue 75 Å the MILES spectral range, the missing flux is reduced by about $\sim 10\%$. This is not surprising given the rapid decay of the U filter transmission at these wavelengths. As expected hot stars require larger corrections, particularly those with temperatures above ~ 10000 K, whilst stars with temperatures below ~ 4000 K show correction factors smaller than 10%. The flux corrections are in the range 10 – 15% for the stars that mainly contribute to the old stellar populations. We obtain separate fits for dwarfs and giants in the MIUSCAT spectral range as follows

$$\begin{aligned} f_U &= -7.4540 + 4.0006T - 0.5254T^2, & T < 3.955, & \text{dwarfs} \\ f_U &= -6.1348 + 2.8159T - 0.3106T^2, & T > 3.955, & \text{dwarfs} \end{aligned} \quad (4)$$

$$\begin{aligned} f_U &= -9.9324 + 5.3528T - 0.7114T^2, & T < 3.895, & \text{giants} \\ f_U &= -7.0157 + 3.2215T - 0.3569T^2, & T > 3.895, & \text{giants} \end{aligned}$$

where T means $\log T_{\text{eff}}$. The total U magnitude is derived by measuring the flux of the MIUSCAT spectrum through the U filter redwards 3464.9 Å and correcting it by the missing flux. These fractions are taken into account during the integration along the isochrone to obtain the corresponding missing flux corrections for the SSP. It is worth noting that these corrections are strictly valid for solar metallicity due to the limited coverage of the Pickles (1998) library in this parameter. However the main contribution to this correction factor comes from the missing spectral range, which represents a small fraction of the total flux in the U band.

2.3 MIUSCAT SSP SEDs

We implement the MIUSCAT stellar library in the models as described in Vazdekis et al. (2010). The spectra of the stars are integrated along the isochrone taking into account their number per mass bin according to the adopted IMF. For this purpose, each requested stellar spectrum is normalized to the corresponding flux in the V band, following our prescription for converting the theoretical parameters of the isochrones to the observational plane, as described in Section 2.1. Note that the latter is performed on the basis of empirical photometric stellar libraries, rather than relying on theoretical stellar atmospheres, as it is usually done in other stellar population synthesis codes. Therefore the SSP SED, $S_\lambda(t, [Z/H])$, is computed as follows:

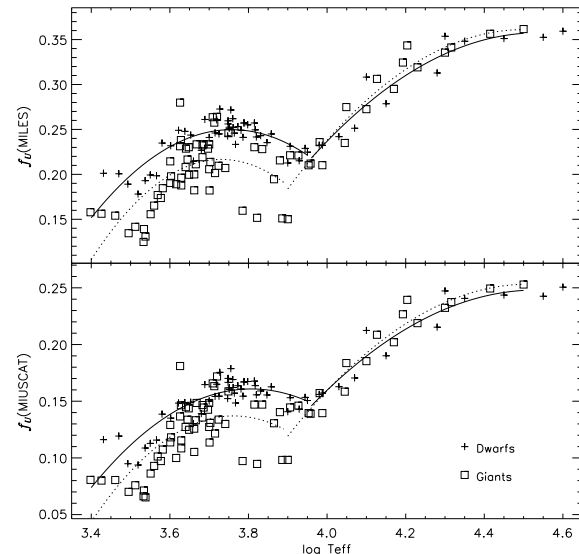


Figure 3. Missing flux correcting factor for the Johnson U filter versus $\log T_{\text{eff}}$ for dwarfs (crosses) and giants (open squares). For this purpose we convolved the U filter response with the low-resolution stellar spectra of the Pickles (1998) library. In the upper panel we show the missing flux factor obtained for the MILES spectral range, whereas in the lower panel we show the one corresponding to the MIUSCAT range. Note that the required correction for the MIUSCAT range is significantly smaller. The fits for dwarfs (solid lines) and giants (dotted lines) are given in Eq. 4.

$$S_\lambda(t, [Z/H]) = \int_{m_1}^{m_t} S_\lambda(m, t, [Z/H]) N(m, t) \times F_V(m, t, [Z/H]) dm, \quad (5)$$

where $S_\lambda(m, t, [Z/H])$ is the empirical spectrum, normalized in the V band, corresponding to a star of mass m and metallicity $[Z/H]$, which is alive at the age assumed for the stellar population t . $N(m, t)$ is the number of this type of star, which depends on the adopted IMF. m_1 and m_t are the stars with the smallest and largest stellar masses, respectively, which are alive in the SSP. The upper mass limit depends on the age of the stellar population. Finally, $F_V(m, t, [Z/H])$ is its flux in the V band. The absolute flux scaling scheme is described in Falc3n-Barroso et al. (2011).

The spectrum of each requested star, with a given set of atmospheric parameters, is synthesized according to the interpolating algorithm described in Vazdekis et al. (2003) and Vazdekis et al. (2010). This code finds the closest stars and weight them according to the distance to the requested point ($\theta_0, \log g_0, [\text{Fe}/\text{H}]_0$) in the stellar parameter space and the signal-to-noise of their spectra. The method is optimized to minimize the errors in case of gaps and asymmetries in the distribution of stars around the requested point. For a full description of the algorithm we refer the reader to Vazdekis et al. (2003) (Appendix B).

We also take into account during the integration along the isochrone the missing fraction of the total flux in the U broad band, i.e. bluewards 3464.9 Å, for each star, f_{U_i} , which

is calculated according to Eq. 4. The resulting fraction for the SSP, $f_{U_{SSP}}$, is then used to correct the flux obtained by convolving the MIUSCAT SSP SED with the response of the U filter. As a test of consistency of these filter measurements, we computed the $f_{U_{SSP}}$ fractions obtained from the SSP SEDs of Bruzual & Charlot (2003) and Maraston (2005) and applied these corrections to the fluxes measured in the MIUSCAT SEDs. The magnitudes computed in the two ways are fully consistent, with difference of the order of 0.01 mag for all the metallicities. This supports our approach of applying the correction factors derived from the solar metallicity stars of the Pickles (1998) library as discussed in Section 2.2.2.

Once an SSP SED based on the MIUSCAT library has been computed we combine it with the original MILES and CaT SSP SEDs of the same age, metallicity and IMF, to construct the final MIUSCAT model SED. For this purpose we follow the same approach described for constructing the composite MIUSCAT stars (see Section 2.2 to recalibrate the models. This approach allows us to keep the MILES and CaT SSP SEDs, which are computed on the basis of these two libraries, untouched (except the smoothing applied to the CaT SED to match the lower resolution of MILES, i.e. 2.51 Å). Although the SSP SEDs computed on the basis of the composite MIUSCAT stars can be safely used in the MILES and CaT spectral ranges, our approach warrants a significantly higher quality in these two ranges as we rely on model computations involving a larger number of stars with better atmospheric coverage. Therefore these new SEDs, which are computed on the basis of the composite MIUSCAT stars, are only used for the wavelength regions that are not covered by the MILES and CaT spectral ranges. In summary, the MILES and CaT spectral ranges contained in the final MIUSCAT SSP SEDs are the ones of Vazdekis et al. (2003) and Vazdekis et al. (2010) SEDs, as updated in this work. An example of a composite MIUSCAT SSP SED is shown in Fig. 4. Table 2.3 summarizes the spectral properties of these models and the SSP parameters for which our predictions can be safely used. The models assume a total initial mass of $1 M_{\odot}$.

For unimodal IMFs with very steep slopes ($\mu > 1.3$) the very low MS stars with $M < 0.5 M_{\odot}$ might have a noticeable impact on the resulting model SEDs, particularly in the redder wavelength ranges (e.g. Vazdekis et al. 1996; Conroy & van Dokkum 2011). In Fig. 5 we show the temperatures and V band magnitudes for three different sets of models: the Girardi et al. (2000) that are employed in this work, the ones of Cassisi et al. (2000) that will be implemented in a forthcoming paper, and those of Pols et al. (1995) that were employed in Vazdekis et al. (1996) models. Note that the models of Girardi et al. (2000) are the hottest ones. Furthermore the obtained discrepancy in temperatures increases with decreasing metallicity. The difference in temperatures between the hottest, i.e. Girardi et al. (2000) and the coolest models, i.e. Pols et al. (1995), are rather similar to those reported in An et al. (2009), when comparing the low-mass stellar models of Girardi et al. (2000) to those implemented in the Dartmouth stellar evolution database (Dotter et al. 2008), i.e. as large as ~ 200 K for solar metallicity. Note however that the obtained differences in the magnitudes of these stars are much less noticeable as is shown in the lower panel of Fig. 5.

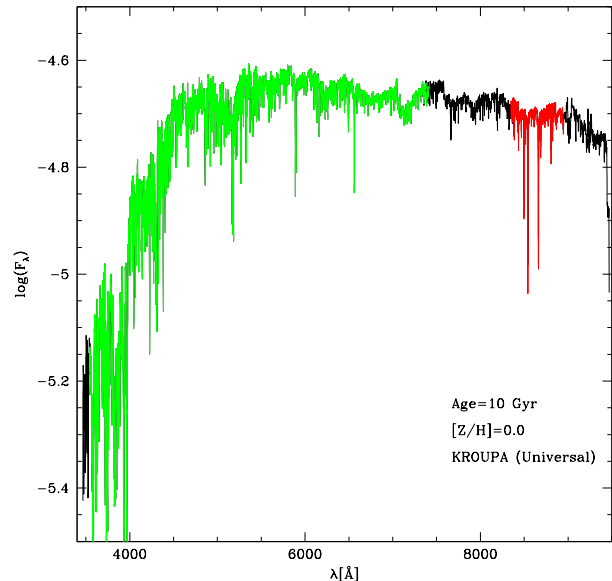


Figure 4. An illustrative example of a MIUSCAT SED corresponding to an SSP of solar metallicity and 10 Gyr, computed with Kroupa Universal IMF. The joined spectra are shown in different colours: green for MILES, red for CaT and black for the Indo-U.S. Note that in the MILES and CaT spectral regions the SEDs are identical to the ones published on the basis of these two libraries, except the fact that the CaT model SED has been smoothed to 2.51 Å (FWHM).

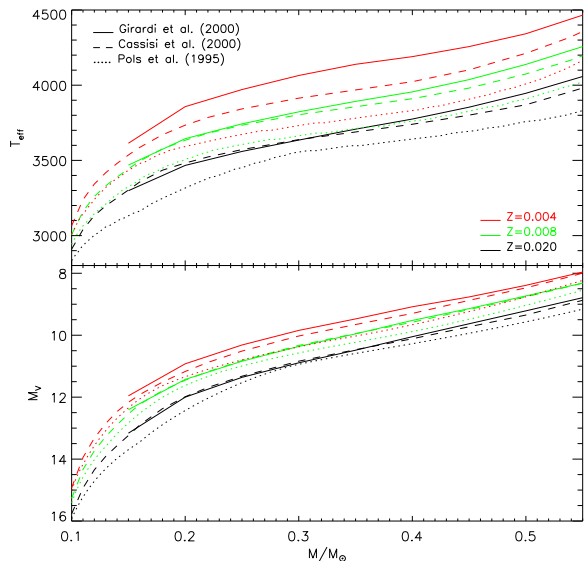


Figure 5. Effective temperatures (upper panel) and V band magnitudes (lower panel) of very low Main Sequence stars for three different set of models and three metallicities, as indicated in the insets of the upper panel.

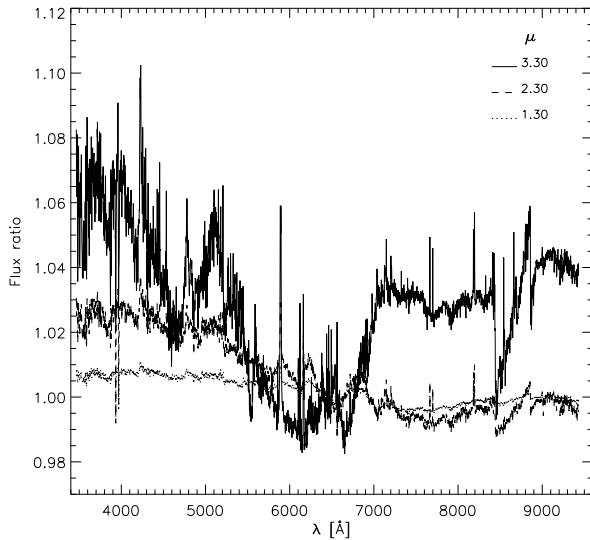


Figure 6. Flux ratio between SSP SEDs, at their nominal resolution, of solar metallicity and 10 Gyr computed with a Unimodal IMF with slopes $\mu = 1.3, 2.3$ and 3.3 , adopting two different models for stars with $M < 0.5 M_{\odot}$ (Girardi et al. 2000; Pols et al. 1995). The spectra were normalized to unity at $\lambda\lambda 6466\text{--}6480 \text{ \AA}$. See the text for details.

To explore the net effect on the synthesized SSP SEDs of adopting different models for these low-mass stars we replaced the stars with $M < 0.5 M_{\odot}$ of Girardi et al. (2000) by those of Pols et al. (1995), i.e. the hottest by the coolest models, respectively. All the stellar models were converted to the observational plane following the same prescriptions described in Section 2.1. Fig. 6 shows the flux ratio between the SSP SEDs of solar metallicity and 10 Gyr with Unimodal IMF of slope 1.3, 2.3 and 3.3, computed with these two sets of stellar models. For $\mu = 1.3$, i.e. the Salpeter case, we do not find any significant effect. For $\mu = 2.3$ the effects are in general smaller than 3%, with the largest impact seen for the Na feature at $\sim 5800 \text{ \AA}$. Following the NaD Lick index definition for this feature (Worthey 1994), the obtained index difference translates to an observing error corresponding to a signal-to-noise around 30. Finally for $\mu = 3.3$ the effects in some features can be as large as $\sim 10\%$, and for that reason we do not consider safe such model SEDs.

To estimate the reliability of the newly computed SEDs and the SSP parameter regions where these models can be considered safe, we use the normalized quality parameter Q_n defined in Vazdekis et al. (2010). To compute Q_n for each SSP we make use of our algorithm for synthesizing a representative stellar spectrum for a given set of atmospheric parameters. The larger the total number of stars and the shorter the distance of their parameters to the requested ones for each star along the isochrone, the larger the quality parameter of the synthesized SSP spectrum is. The obtained value is normalized with respect to a minimum acceptable value, which comes from a poor, but still acceptable, parameter coverage of the stellar library. We refer the interested reader to Vazdekis et al. (2010) for a full description of the method. Q_n allows us to obtain a quality measure of the SSP SED, due to the atmospheric parameter coverage of the stellar library feeding the models.

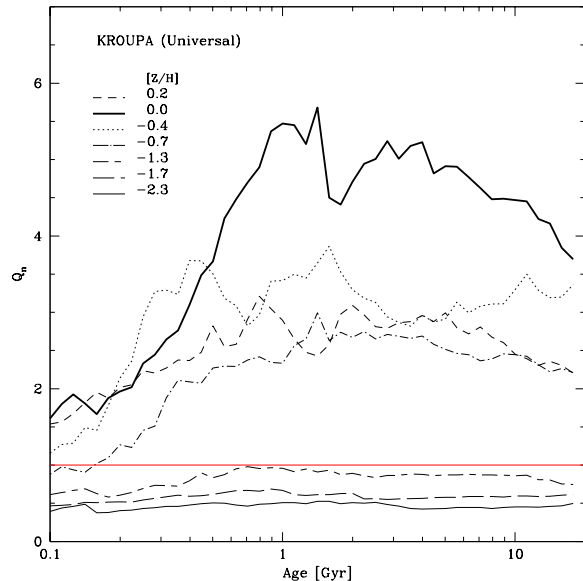


Figure 7. The quality parameter, Q_n , defined in Vazdekis et al. (2010) as a function of the SSP age (in Gyr) for different metallicities, indicated by the line types as quoted in the inset. For computing the SEDs we use a Kroupa Universal IMF. SSPs with Q_n values larger than 1 can be safely used (see the text for details).

Figure 7 shows the value of Q_n as a function of the SSP age (in Gyr) for different metallicities (different line types) and adopting a Kroupa Universal IMF. SSP SEDs with Q_n values above 1 can be considered of sufficient quality, and therefore they can be safely used. Note that these values only apply to the spectral ranges not covered by MILES and CaT SEDs, which in general provide larger values. As expected, the higher Q_n values are obtained for solar metallicity. Q_n reaches a value of ~ 5 for stellar populations in the range 1 – 10 Gyr. Outside this age range the quality decreases as low-mass and hotter MS stars are less numerous in the MIUSCAT database (see Fig. 2). Both, for the supersolar and for the low metallicities we obtain lower, but acceptable, values. For $[Z/H] = -1.31$ we obtain Q_n values that are slightly below 1, but should not be considered safe, particularly for detailed spectroscopic studies that employ line-strengths or full spectrum-fitting approach. Finally, for lower metallicities the MIUSCAT SEDs are not reliable, though these models might still be used for some applications such as, e.g., broad-band colours (see Section 3). Note that in general the Q_n values obtained for the MIUSCAT SEDs are lower than those of MILES SEDs (see second panel of Fig. 6 in Vazdekis et al. 2010), for which we obtain acceptable Q_n values for metallicities as low as $[Z/H] = -2.3$. Table 2.3 summarizes the safe ranges for the MIUSCAT SED spectral ranges that are not covered by MILES and CaT SEDs. For the latter we refer the reader to Vazdekis et al. (2010) and the MILES webpage.

Table 2. Spectral properties and parameter coverage of the SSP SEDs

Spectral properties	
Spectral range	$\lambda\lambda$ 3464.9 – 9468.8 Å
Spectral resolution	FWHM = 2.51 Å, ($\sigma = 64.1$ km s ⁻¹ at 5000 Å, $\sigma = 40.1$ km s ⁻¹ at 8000 Å)
Linear dispersion	0.9 Å/pix (54.0 km s ⁻¹ at 5000 Å, 33.7 km s ⁻¹ at 8000 Å)
Continuum shape	Flux-scaled
Units	$F_\lambda/L_\odot \text{Å}^{-1} M_\odot^{-1}$, $L_\odot = 3.826 \times 10^{33} \text{erg.s}^{-1}$
SSPs parameter coverage	
IMF type	Unimodal, Bimodal, Kroupa universal, Kroupa revised
IMF slope (for unimodal and bimodal)	0.3, 0.8, 1.0, 1.3, 1.5, 1.8, 2.0, 2.3, 2.8, 3.3
Stellar mass range	0.1 – 100 M_\odot
Metallicity	-2.32, -1.71, -1.31, -0.71, -0.41, 0.0, +0.22
Age	$0.06 < t < 18$ Gyr
SAFE SSP SEDs for non MILES/CaT spectral ranges	$(-0.71 \leq [Z/H] \leq +0.22 \ \& \ 0.06 < t < 18 \text{ Gyr} \ \& \ \mu \leq 2.3)$

3 BEHAVIOUR OF THE MODELS

The behaviour of our model SEDs as a function of the SSP parameters in the CaT and MILES wavelength ranges have been shown in Vazdekis et al. (2003) and Vazdekis et al. (2010). We refer the reader to these papers for an extensive analysis. In this section we focus on the new additions from expanding the spectral coverage of the model SEDs. Among these new features we discuss here our colour measurements, which are obtained from convolving the MIUSCAT SSP SEDs with the corresponding filter responses.

Fig. 8 shows the broad-band Johnson-Cousins (Buser & Kurucz 1978; Cousins 1980) colours, $U - B$, $B - V$, $V - R$ and $V - I$, derived from the MIUSCAT SSP SEDs for different ages and metallicities, adopting a Kroupa Universal IMF with the zero point set with the Vega spectrum of Hayes (1985). For comparison we also show the photometric colours of Vazdekis et al. (1996), as updated in Vazdekis et al. (2010), which are calculated on the basis of the relations described in Section 2.1, which come from extensive empirical photometric libraries. In this figure $B - V$ is the only colour that can be fully measured within the MILES spectral range, with no need to use the MIUSCAT wavelength range extension.

In general we see that the obtained residuals are as small as typical zero-point uncertainties (~ 0.02 mag) for nearly all the metallicities for the $B - V$, $V - R$ and $V - I$ colours. For the $B - V$ colour this can be attributed to the very high flux-calibration quality of the MILES stellar spectra as was shown in Sánchez-Blázquez et al. (2006). On the other hand the good agreement obtained for the $V - R$ and $V - I$ colours should be attributed to our method for scaling and joining the different spectral ranges. Finally the largest residuals are obtained for the $U - B$ colour. Note however that the measurement of the U magnitude is very sensitive to the various filter definitions for this band as is shown in Paper II. Our photometric $U - B$ predictions are mainly obtained with the aid of the relations of Alonso et al. (1996, 1999), as for the other filters. However these $U - B$ relations are not completely homogeneous with the relations obtained by these authors for the other filters. We refer the interested reader to these authors for a detailed description of the methods to derive these relations.

Another interesting aspect that can be studied with the

newly synthesized MIUSCAT SSP SEDs is the variation of the colours and spectral features with the IMF, due to the expanded spectral range. The first row of panels of Fig. 9 shows the ratio obtained by dividing the SSP SEDs of solar metallicity and various IMFs with respect to the SED computed with a Unimodal IMF of slope 1.3 (Salpeter case), for two different ages (2 and 10 Gyr). All the spectra are smoothed to 5 Å (FWHM), i.e. the constant resolution that characterizes the LIS-5.0 Å system of index measurements introduced in Vazdekis et al. (2010). The first panel shows that the models constructed with a Kroupa Universal IMF is rather similar to the Salpeter case for the two ages. The larger, though small, difference is only seen for redder wavelengths for the 10 Gyr old model. This colour trend is further accentuated for the IMF with the largest slope ($\mu = 2.3$), i.e., the larger the slope the larger the effect is. Also, the effect is more pronounced as the age increases.

This effect is originated by the large contribution of low-mass MS stars in the steep IMF models. Being their SEDs red, the resulting total flux of the model is redder than models with flatter IMF slopes. Unlike the blue colours, the redder ones are clearly sensitive to the IMF. A similar result was shown in Vazdekis et al. (1996).

Apart of the colours we also see in the bottom panels a significant IMF-sensitivity for various absorption spectral features and molecular bands. Among the most prominent features we identify the Ca H & K around ~ 3950 Å, Ca I at ~ 4227 Å, the Na I doublets at ~ 5900 Å and ~ 8200 Å, H α and the Ca II triplet around ~ 8600 Å. The IMF-sensitivity of all these features, and other features in redder wavelengths, have been recently discussed in Conroy & van Dokkum (2011) (see references therein). We also find emphasized IMF-sensitivities in the TiO molecular bands redwards 5900 Å. These include the prominent features seen at ~ 5950 Å, ~ 6200 Å, ~ 6600 Å, ~ 7200 Å and ~ 8900 Å. The first two TiO bands are included in the Lick system of indices (i.e., TiO₁ and TiO₂) (Worthey94). Indices for the other TiO bands have been discussed and modelled for stellar populations in e.g., Schiavon et al. (1997), Faber & French (1980) and Vazdekis et al. (2003). Moreover the slope of the SSP SED around the Ca II triplet at ~ 8600 Å has also been shown to be sensitive to the IMF slope (Vazdekis et al. 2003; Cenarro et al. 2009). In the latter paper this slope has been modelled by defining a specific

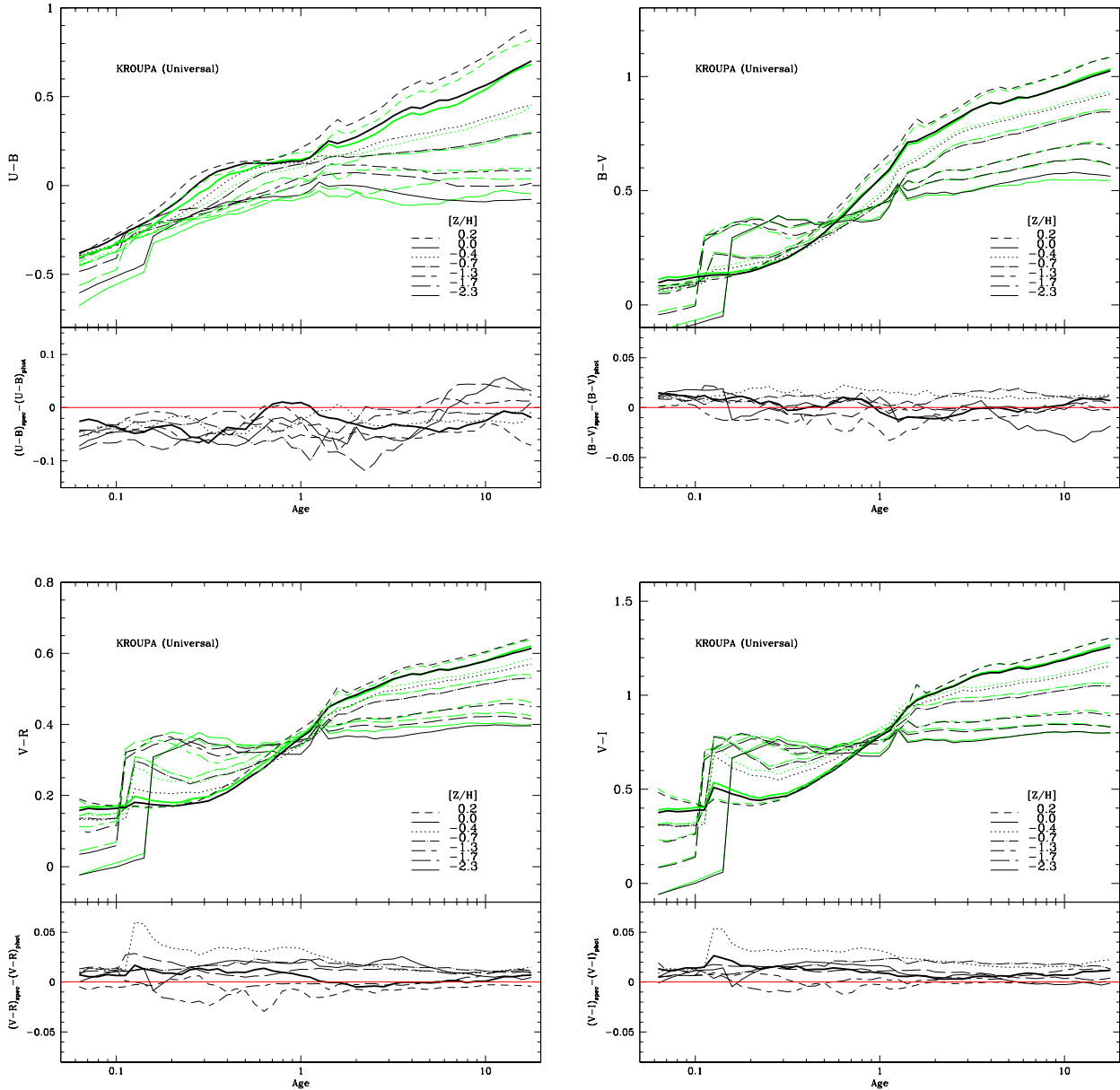


Figure 8. We plot the synthetic broad band $U-B$, $B-V$, $V-R$ and $V-I$ colours (black lines) derived from the MIUSCAT SSP SEDs for different ages and metallicities (as indicated within the panels) and the Kroupa Universal IMF with the zero point set with Hayes (1985) Vega spectrum. The green lines represent the photometric colours computed by Vazdekis et al. (1996), as updated in Vazdekis et al. (2010), which are calculated on the basis of the empirical photometric relations described in Section 2.1. The obtained residuals are also shown for each colour.

index, named sTiO. An index-index diagram, which includes this index and the CaII triplet at $\sim 8600 \text{ \AA}$, has been proposed in Cenarro et al. (2003) to diagnose the IMF slope.

It is worth noting that whereas the CaII triplet decreases with increasing IMF slope, the nearby NaI doublet at $\sim 8200 \text{ \AA}$ increases. Therefore the study of these two features constitutes a powerful diagnostic for constraining the IMF. The latter feature, which falls in the spectral region not covered by the MILES and CaT models, represents a very important improvement of the newly synthesized MIUSCAT SSP SEDs. We focus on this aspect in Section 4.2. The sen-

sitivity of the CaII triplet to the IMF in SSP models was extensively shown and discussed in Vazdekis et al. (2003). See also Schiavon et al. (2000) and Conroy & van Dokkum (2011). The IMF-sensitivity of the NaI doublet at $\sim 5900 \text{ \AA}$ was also shown in Vazdekis et al. (1996), Schiavon et al. (2000) and Conroy & van Dokkum (2011).

As expected, the flux ratio features that are seen at 5 \AA resolution are generally less pronounced when the spectra are smoothed to match the lower resolution of the LIS-14.0 \AA system, i.e. $\text{FWHM}=14 \text{ \AA}$, as shown in the second row of panels of Fig. 9. This extent shows that the resolution of

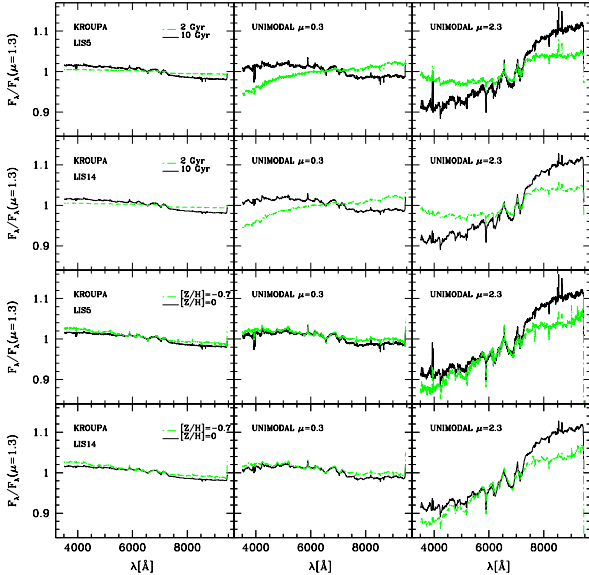


Figure 9. Flux ratio between SSP models with various IMFs (Kroupa Universal in the left panels, Unimodal with slope $\mu = 0.3$ in the center and Unimodal with slope $\mu = 2.3$ in the right) with the corresponding model with Unimodal IMF and $\mu = 1.3$ (i.e. Salpeter). The first row of panels shows models with solar metallicity and two ages (2 and 10 Gyr), as indicated in the legend of the left panel. All the models were smoothed to match the resolution of the Vazdekis et al. (2010) LIS-5.0Å line-index system, i.e. FWHM=5.0Å. The spectra were normalized to unity at $\lambda \sim 6466-6480$ Å. We keep the same scale for all the flux ratios. The second row of panels shows the same flux ratios but with the SSP SEDs smoothed to match the spectral resolution of the LIS-14.0Å system of Vazdekis et al. (2010), i.e. FWHM=14 Å. Finally, the third and fourth row of panels show the flux ratios of SSP SEDs with 10 Gyr and two metallicities ($[Z/H]=0.0$ and $[Z/H]=-0.7$), as indicated in the legend of the first panel, with all the models smoothed to match the LIS-5.0Å and LIS-14.0Å systems, respectively.

the data or the velocity dispersion of the galaxies should be taken into account when studying the IMF effects.

In the third and fourth row of panels of Fig. 9 we fix the age of the SSP SEDs to 10 Gyr in order to study the IMF sensitivity as a function of the metallicity at the resolutions of the LIS-5.0Å and LIS-14.0Å systems, respectively. Overall we see that most of the flux ratio features tend to be less pronounced in the metal-poor model. Interestingly, this is not the case for the NaI doublet at ~ 8200 Å.

In Fig. 10 we show the difference in $B - V$ and $V - I$ colours with respect to the corresponding values for the models with Unimodal IMF with $\mu = 1.3$ as a function of the IMF slope, for the two ages and two metallicities. As it can be inferred from Fig. 9, which shows the larger IMF-sensitivity of the redder spectral regions, the $V - I$ colour differences are significantly larger than those obtained for $B - V$. We also see that the main increase of the colour difference takes place for IMFs with $\mu > 2$. Finally, a similar behaviour is found for the colours of the SDSS filters as shown in Fig. 11.

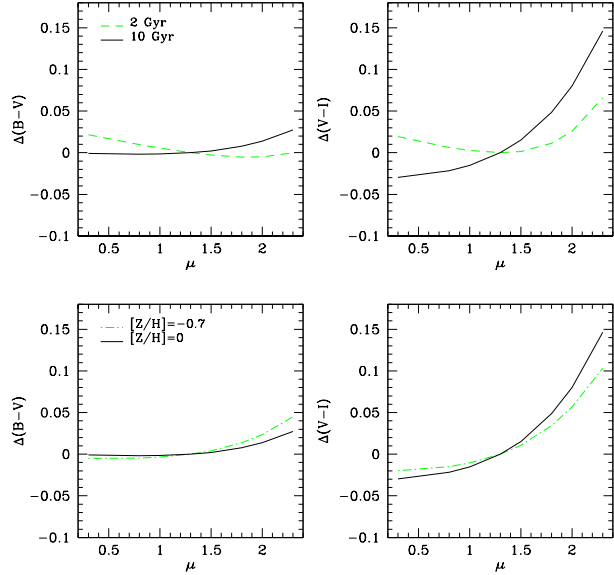


Figure 10. $B - V$ (left panels) and $V - I$ (right panels) colour difference with respect to the SSP models with Unimodal IMF with $\mu = 1.3$ (i.e. Salpeter), as a function of the IMF slope. In the upper panels two ages (2 and 10 Gyr) are considered, whereas in the lower panels we show the results for two metallicities ($[Z/H]=-0.7$ and 0).

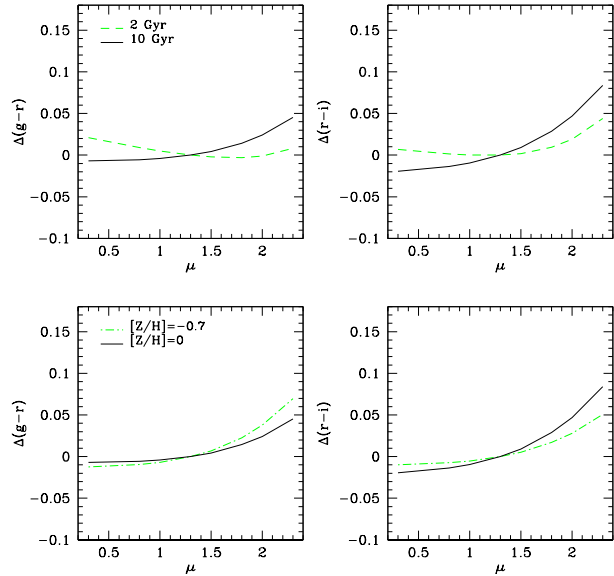


Figure 11. Same as in Fig. 10 but for the $g - r$ (left panels) and $r - i$ (right panels) colours of the SDSS system.

4 APPLICATIONS

In this section we show several applications to illustrate the potential use of MIUSCAT SSP SEDs. We only focus on those colours and features that we were not able to measure with the MILES/CaT SEDs but are now possi-

ble with the present extension of the spectral coverage of the models. These examples include broad-band colours, a newly-defined line-strength spectroscopic absorption index and survey-oriented spectrophotometric applications.

4.1 Galactic globular cluster colours

Fig. 12 shows a comparison of the $V - R$ and $V - I$ colours with the Milky Way globular cluster data with $E(B - V) < 0.1$, from the catalog of Harris (1996). The colours are plotted against metallicities from the same catalog. All the models have ~ 12 Gyr and adopt a Salpeter IMF. We provide two flavours of models: the photometric predictions of Vazdekis et al. (1996), as updated in Vazdekis et al. (2010), and the synthetic colours derived from the MIUSCAT SEDs. We see that these two sets of predictions agree very well each other, matching the observations for the expected ages and metallicities according to independent measurements from CMD studies. We also show for comparison the colours from the models of Bruzual & Charlot (2003) and Maraston (2005). The latter provide too red values in comparison to our predictions and the data. Maraston & Strömbäck (2011) have shown that models employing theoretical stellar libraries tend to provide such redder colours in comparison to those based on empirical libraries, as in the present work.

Further colour comparisons for globular clusters in the Galaxy and in M 31 are shown in Paper II. Both colours in the Johnson-Cousins and in the SDSS systems are discussed. We also show in that paper an extensive and comprehensive study for the early-type galaxies of the SDSS out to $z \sim 0.5$.

4.2 Line-strength index definitions

We illustrate in this section the potential use of the MIUSCAT SSP SEDs for defining new line-strength indices. For this purpose we focus on the most interesting feature that can be found in the spectral region that was not covered by the MILES and CaT SEDs, i.e., the NaI doublet at ~ 8200 Å (see Section 3). This feature, together with the FeH Wing-Ford band absorption at 9916 Å, has been recently used to suggest a dwarf-enriched scenario for massive cluster elliptical galaxies (van Dokkum & Conroy 2010). There is also evidence of NaI gradients suggesting concentrations of metal-rich dwarfs toward the centers of giant galaxies (Carter, Visvanathan & Pickles 1986).

We follow here the same scheme used to define the Lick-style indices of the optical spectral range (Worthey 1994). We use a feature bandpass and two pseudocontinua bandpasses, which are located at either side of the feature, in order to establish the flux level of the continuum at the feature. These bandpasses are illustrated in Fig. 13, whereas the limiting wavelengths are listed in Table 3. This is a modified version of the index proposed for this feature by Schiavon et al. (1997) that avoids the TiO bandhead absorption at 8205 Å, which becomes increasingly stronger than the NaI lines for decreasing temperatures in giants (see also Carter, Visvanathan & Pickles 1986). Our index represents an improvement over previous definitions in this respect (e.g., Faber & French 1980, Serven, Worthey & Briley 2005; Conroy & van Dokkum 2011). In fact Alloin & Bica (1989) propose an alternative discussion about dwarf/giants star

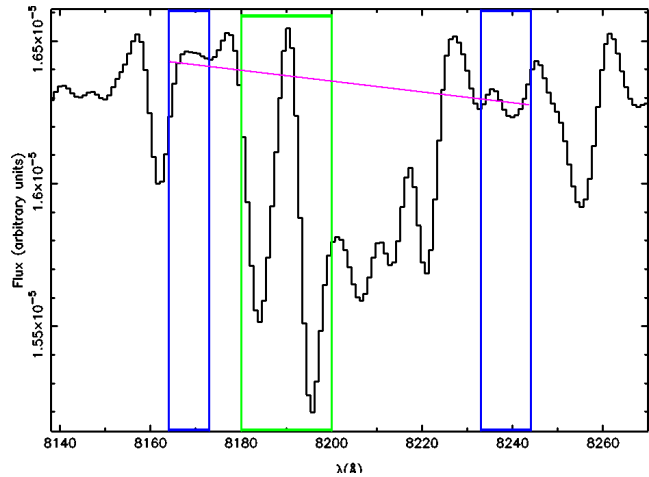


Figure 13. New index definition for the NaI doublet around 8200 Å (NaI8200A). The feature bandpass is indicated in green. The continuum flux level (dashed magenta line) is defined by the pseudocontinua at either side of the feature (indicated in blue). The plotted SED corresponds to a MIUSCAT SSP model of solar metallicity, 10 Gyr and Unimodal IMF with slope 1.3 (i.e. Salpeter). The spectrum has been smoothed to match the spectral resolution of the LIS-5.0 Å line-index system, i.e., 5 Å (FWHM).

content in the semi-stellar nucleus of M 31, which is based on the metallicity, precisely due to the TiO absorption contamination. Note however that our index definition is certainly an advantage when fitting low velocity dispersion galaxies as this contamination cannot be avoided in more massive systems. Another advantage of the NaI8200A index is that we adopt a significantly wider pseudocontinua (~ 10 Å) than in the Schiavon et al. (1997) index (< 1 Å), which makes it more robust against the signal-to-noise of the observational data.

It is worth noting that we do not intend here to provide an optimal index definition that requires a specifically dedicated paper, which is out of the scope of this work. A good example can be found in Cervantes & Vazdekis (2009), where we proposed a new index for the $H\beta$ feature, with an unprecedented ability to disentangle the age of the stellar populations. Nonetheless, we have tried several index definitions for this feature, which turned out to be extremely sensitive to the velocity dispersion smearing of the two absorption lines of this doublet. In fact these lines blend in a single feature for velocity dispersions around 200 km s^{-1} . Therefore it is important to assess its dependence on this effect if this feature were to be used for constraining the IMF. Our experiments show that the index definition is more robust against such smearing if these two lines are included within the feature bandpass. Note also that our feature bandpass is well isolated from the two selected pseudocontinua bandpasses. Fig. 14 shows the behaviour of the NaI8200A index against the velocity dispersion for models with Unimodal IMF and varying slope. The plots show the results for two different ages and solar metallicity, but similar patterns are seen for other values of these two SSP parameters. As expected, we see that the index decreases its strength with decreasing resolution, but this dependence does not vary significantly with the IMF slope.

Although not shown here, we also find that the

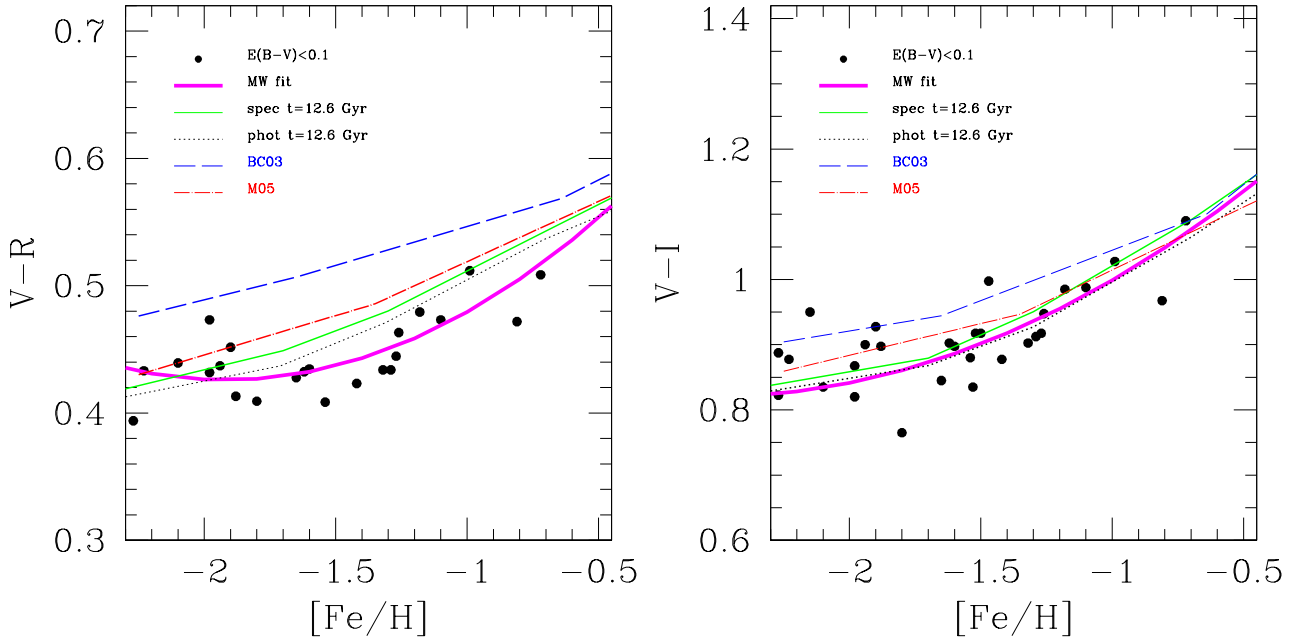


Figure 12. Comparison of $V - R$ (left panel) and $V - I$ (right panel) colours from models of ~ 12 Gyr and MW globular cluster data from the Harris (1996) catalog. We only plot clusters with small extinction values ($E(B - V) < 0.1$). The colours are plotted against the metallicity from the same catalog. The thick magenta line represents an order 2 polynomial fit to the data. All the models are computed adopting a Salpeter IMF. In each panel the dotted black line represents the photometric colour prediction of Vazdekis et al. (1996), as updated in Vazdekis et al. (2010), whereas the thick solid green line represents the synthetic colour derived from the MIUSCAT SEDs. We also show for comparison the Bruzual & Charlot (2003) and Maraston (2005) models in long-dashed blue and dot-dashed red lines, respectively.

Table 3. Bandpass limiting wavelengths for the NaI8200A index.

Feature bandpasses (\AA)	Pseudo-continuum bandpasses (\AA)
8180–8200	8164–8173
	8233–8244

NaI8200A index is extremely robust against uncertainties in the spectrum shape, which might result from, e.g., flux-calibration issues. The differences in strengths obtained from measuring the index in both an SSP SED with solar metallicity and 13 Gyr with flux-calibrated response and the same model SED after removing its continuum is virtually nil. This is expected as the index definition encompasses only 80 \AA , i.e. from the bluest wavelength of the blue pseudocontinuum to the reddest wavelength of the red pseudocontinuum.

Fig. 15 shows the behaviour of the NaI8200A index as a function of age and metallicity for SSP SEDs with Unimodal IMF with two different slopes, $\mu = 1.3$, i.e. Salpeter, and steeper, $\mu = 2.3$. We use for these measurements the LIS-14.0 \AA system defined in Vazdekis et al. (2010). This system has a flux-calibrated response curve and a constant resolution, $\text{FWHM} = 14 \text{ \AA}$, along the whole spectral range. At $\sim 8200 \text{ \AA}$, where this feature is located, this resolution translates to $\sigma \sim 220 \text{ km s}^{-1}$, which is appropriate for massive galaxies. Although the NaI8200A index depends on the metallicity and age, it is particularly sensitive to the IMF slope, as expected from Fig. 9. These results are in good agreement with Schiavon et al. (2000). Fig. 15 also shows

that the sensitivity to the IMF increases with increasing age and decreasing metallicity. According to the formalism of Cardiel et al. (1998) we obtain for this index an error of ~ 0.2 with a $S/N(\text{\AA}^{-1}) \sim 30$, for an old and solar metallicity model. Such error is similar to the index difference obtained when varying the IMF slope from 1.3 to 2.3 (see Fig. 15). This shows that to apply this index for constraining the IMF in massive galaxies we require spectra with significantly higher S/N. Note however that such IMF sensitivity might be masked by similar index variations due to $[\text{Na}/\text{Fe}]$ abundance ratio, as shown in Conroy & van Dokkum (2011). These authors studied the sensitivity of this feature to both $[\text{Na}/\text{Fe}]$ and $[\alpha/\text{Fe}]$ abundances in SSP models of 13 Gyr.

As it can be seen from Fig. 9 and Fig. 15 this feature strengthens with increasing IMF slope, whilst the CaII triplet at $\sim 8600 \text{ \AA}$ weakens. This extent has been noted by Schiavon et al. (2000) and Conroy & van Dokkum (2011). In the latter it is shown that an increase in $[\text{Na}/\text{Fe}]$ causes a decrease in the strength of the CaII triplet, as Na is a major contributor to the electron pressure in late-type stars. In Vazdekis et al. (2003) we fully characterize the behaviour of the CaII triplet in SSPs. Therefore these two features can be used to propose an index-index diagnostic diagram to constrain the IMF. Fig. 16 shows the resulting model grids for two different ages (2 and 12.6 Gyr) for models with Unimodal IMF. A range of IMF slopes and metallicities is shown. All the index measurements are performed on the LIS-14.0 \AA system. These grids allow us to distinguish the IMF slope if the age and the $[\text{Na}/\text{Fe}]$ abundance ratio are properly constrained.

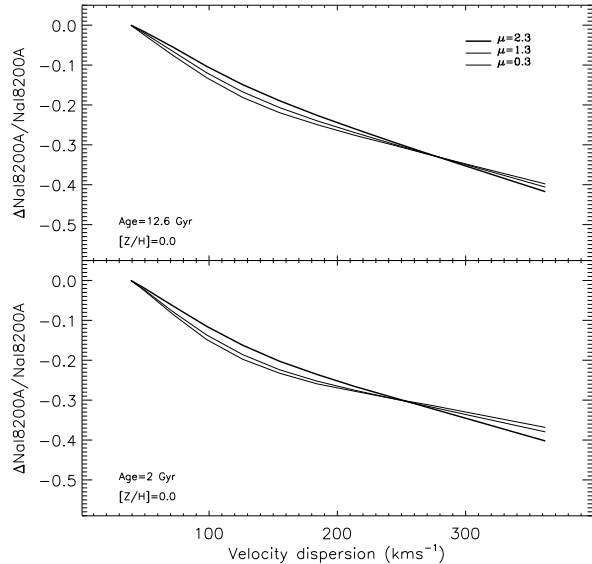


Figure 14. Broadening correction for the newly defined NaI8200A index, $\Delta\text{NaI8200A}/\text{NaI8200A}$, in SSPs with Unimodal IMF and varying slopes. The solid lines become thicker with increasing slope. The upper panel shows the results for a 12.6 Gyr model, whereas in the lower panel we show the results for a 2 Gyr, the two for solar metallicity. We have broadened the model spectra by convolving with gaussians from the nominal resolution, i.e. $\sigma=39 \text{ km s}^{-1}$ (FWHM=2.51 Å) at 8200 Å, up to $\sigma=360 \text{ km s}^{-1}$, in steps of 30 km s^{-1} .

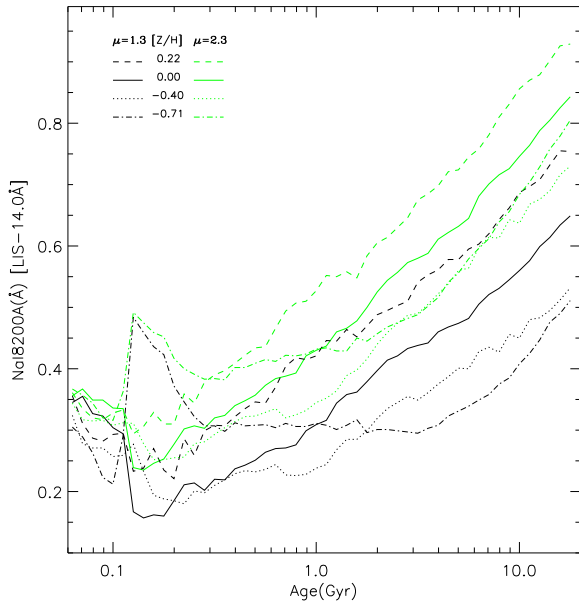


Figure 15. Behaviour of the NaI8200A index as a function of age for SSP models of different metallicities, as indicated in the legend, for a Unimodal IMF with slope $\mu = 1.3$ (Salpeter) and $\mu = 2.3$, plotted in black and green lines, respectively. All the index measurements are performed in the LIS-14.0Å system (FWHM=14 Å).

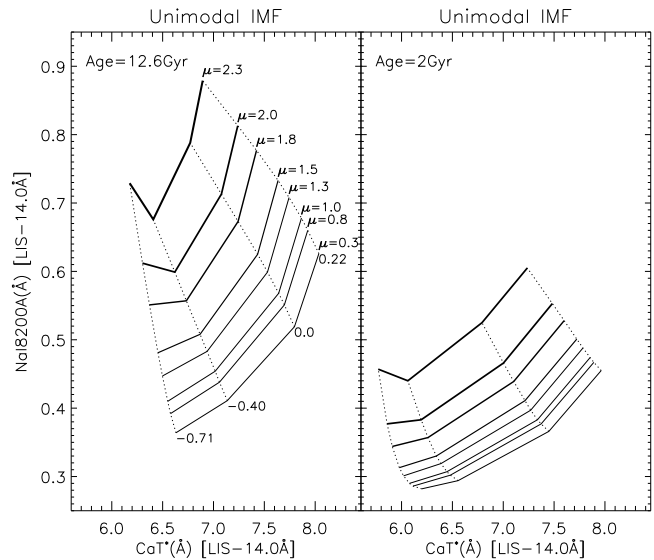


Figure 16. NaI8200A vs. CaT* diagnostic diagram to constrain the IMF slope. We adopt a Unimodal IMF for all the models. The CaT* index is defined in Cenarro et al. (2001). The solid lines indicate models with constant IMF slope, the thicker the line the higher the slope ($\mu = 0.3, 0.8, 1.0, 1.3, 1.5, 1.8, 2.0, 2.3$). The dotted lines represent models of constant metallicity ($[Z/H] = -0.71, -0.40, 0.0, 0.22$). The metallicity and IMF slope values are quoted in the left panel, where we show the grid corresponding to models of 12.6 Gyr. In the right panel we show the grid for 2 Gyr. All the index measurements are performed in the LIS-14.0Å system.

4.3 Galaxy spectrophotometric surveys

The use of multi-filter photometric surveys to determine SEDs and redshifts with high enough level of accuracy (SDSS, see also COMBO-17: Wolf et al. 2008; COSMOS: Ilbert et al. 2009; ALHAMBRA: Moles et al. 2008) has opened a new way to analyze the stellar populations of galaxies at different z -values and in different environments, thus allowing for the study of the evolution of galaxies and cosmology using huge samples.

One of the major advantages of this kind of surveys is the fact that they provide low resolution spectroscopy for every pixel of the sky. With low resolution spectrophotometric data, spectral fitting techniques over the full spectral range are mandatory to exploit as much as possible the information in the data. A unique characteristic of this type of data is the fact that the photo-spectra constructed on the basis of single narrow-band filter imaging does not suffer from flux calibration systematic uncertainties, unlike standard spectroscopy. Every single point of the photo-spectrum -i.e. every filter- is observationally independent of the rest of the photo-spectrum, so the resulting SED is not affected by large scale systematics in the relative flux calibration (hence in the SED colors). With this unique advantage in mind, for the proper analysis of the SEDs of galaxies and stars it is crucial to use template stellar libraries with extremely accurate flux calibration, like MIUSCAT. In this sense, MIUSCAT, and all the SED SSP models derived from this library, are perfectly suited for the analysis and interpretation of op-

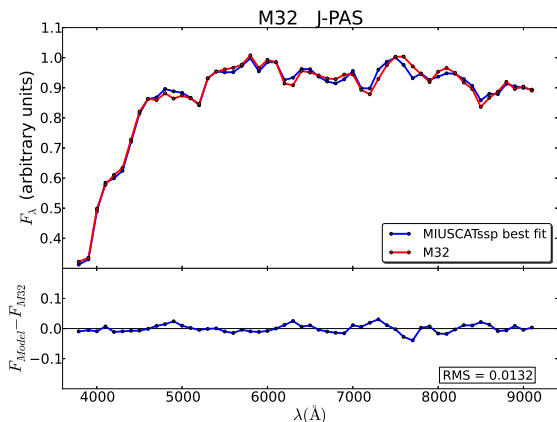


Figure 17. Spectral fitting of M32 using the MIUSCAT SSP SEDs. The spectrum of the galaxy at the J-PAS resolution is plotted in red. The best MIUSCAT SSP fit (Age = 4.6 ± 1.1 Gyr; $[Z/H] = 0.04 \pm 0.08$ dex) to the spectrum of M32, as derived from a standard χ^2 minimization technique, is plotted in blue. The residuals are shown in the lower panel with the same scale. See the text for more details.

tical spectrophotometric data, provided the accurate flux calibration of the library stars and the full optical spectral coverage.

To illustrate a possible use of these new models, we focus on a test-case based on the Javalambre-PAU Astrophysical Survey (J-PAS: Benítez et al. 2009; Cenarro et al. 2010), a new survey with 54 narrow-band (100 Å) contiguous optical filters ($\lambda \sim 3500 - 9500$ Å) under preparation at the Observatorio Astrofísico de Javalambre, which will provide low resolution ($R \sim 30$) spectrophotometric data for hundred million galaxies. Figure 17 illustrates the best SED fitting derived for the integrated spectrum of M32 from Bica, Alloin, & Schmidt (1990), taken from the compilation of Santos et al. (2002), using the MIUSCAT SSP models as input templates. M32 and the template spectra have been convolved with the J-PAS filters to simulate a real case. It is clear from the figure that the best fit, derived from a standard χ^2 minimization technique, reproduces well the observed spectrum at both low and high frequencies. The obtained residuals are shown in the lower panel. Note the telluric absorption still present in the data in the spectral range $\lambda \sim 7000 - 8000$ Å. The best solution corresponds to a MIUSCAT SSP model of 4.6 ± 1.1 Gyr and around solar metallicity (0.04 ± 0.08 dex), in good agreement with results based on much higher resolution spectroscopic data (e.g. Vazdekis & Arimoto 1999; Schiavon, Caldwell, & Rose 2004).

5 THE WEB TOOL

The extension of the spectral range of our models based on the composite MIUSCAT stellar spectra allows us to cover the gap left by our previous model predictions based on the MILES and CaT libraries, as well as to extend blueward and redward these libraries the wavelength coverage. Therefore this extension represents a significant improvement that could be useful for many applications as well as for model

comparisons. To facilitate the exploitation of these models we have integrated these new predictions within our recently developed website (<http://miles.iac.es>). This web provides the necessary support for using these model SEDs as well as those predictions based on MILES, CaT and Jones (1999) stellar library.

All these models as well as the MILES and CaT stellar libraries can be retrieved and handled according to the requirements of the users. The webtools include the transformation of the spectra to match the instrumental set-up of the observations (spectral resolution and sampling), measurements of line-strength indices and synthetic magnitudes derived from the spectrum. Further descriptions of all these applications are described in Paper II.

6 SUMMARY AND CONCLUSIONS

We have extended the spectral coverage of our stellar population synthesis models by combining the predictions based on the MILES (Sánchez-Blázquez et al. 2006), CaT (Cenarro et al. 2001) and Indo-U.S. (Valdes et al. 2004) empirical stellar spectral libraries. For this purpose we combined the stellar spectra of these three libraries for a subsample of 432 stars of the Indo-U.S. database, with no gaps in the relevant spectral regions and with no significant telluric absorption residuals. However the whole Indo-U.S. stellar database was taken into account for matching the stellar parameters of this library to the MILES/CaT system. Due to the limited flux-calibration quality of the spectra of the Indo-U.S. library, we used the MILES and CaT spectra as a reference. We scaled these two spectral ranges according to empirical relations between the stellar parameters and the Johnson-Cousin $V - I$ colour, which are based on extensive photometric stellar libraries (mainly Alonso et al. 1996 for dwarfs and Alonso et al. 1999 for giants). The same prescriptions were employed to convert the theoretical parameters of the stellar isochrones (Girardi et al. 2000) that feed the models to observable fluxes and colours. For the selected Indo-U.S. stars that are lacking in either the MILES or CaT databases, or in the two, we synthesized the corresponding stellar spectra for the same atmospheric parameters using the MILES and CaT interpolators described in (Vazdekis et al. 2010) and (Vazdekis et al. 2003), which are also employed to generate the required spectra to populate the isochrones during the SSP SED calculations.

Appart of filling-in the spectral gap between the MILES and CaT libraries the Indo-U.S. stellar spectra allowed us to slightly extend bluewards MILES and redwards CaT the spectral ranges of these two libraries. Finally the spectral ranges covered by the Indo-U.S. and CaT stellar libraries have been smoothed and resampled to match the values of MILES. The resolution is therefore constant along the whole spectral range, i.e. 2.5 Å (FWHM), with 0.9 Å per pixel. The spectral coverage of the composite stellar spectral range is $\lambda \sim 3464.9 - 9468.8$ Å.

The composite MIUSCAT stellar spectra were implemented in our models to compute SSP SEDs based on these spectra. These models were then combined with the published model SEDs for the MILES (Vazdekis et al. 2010) and CaT (Vazdekis et al. 2003) following a similar approach to that employed for the MIUSCAT stars, keeping the SSP

flux scaling for these two spectral regions. Therefore in the composite MIUSCAT SSPs the SEDs in the MILES and CaT spectral ranges are identical to the originally published models, with the exception of the resolution of the CaT models, which have been smoothed to match that of MILES. We estimated the reliability of the resulting models according to the method described in Vazdekis et al. (2010), which takes into account the atmospheric parameter coverage of the 432 stars included in the MIUSCAT stellar library. The new model SEDs are reliable in the metallicity range ($-0.71 \leq [Z/H] \leq 0.22$) for all the ages (0.063 – 17.8 Gyr) and IMF shapes (Unimodal, Bimodal, Kroupa Universal and Kroupa Revised, as described in Vazdekis et al. (2003)) and IMF slopes ($0.3 \leq \mu \leq 2.3$) that are considered in this work. Broad band colours are also acceptable outside these ranges.

The new models allow us to measure colours involving the Johnson-Cousins and SDSS broad-band filters from U to I and from u to i , respectively. To measure the magnitude in the U filter we compute a correction factor for the missing flux, as this filter extends bluewards the MIUSCAT spectral range. This correction is computed with the aid of the Pickles (1998) low-resolution stellar library. The good flux-calibration quality of the resulting model spectra allows us to measure accurate colours in the covered spectral range. The derived SSP colours are in very good agreement with the corresponding predictions obtained on the basis of empirical relations between colours and stellar parameters, which come from extensive photometric libraries.

These model SEDs can be particularly useful for galaxy surveys, allowing to study the behaviour of the model SEDs with relevant stellar population parameters for a variety of filter responses.

Unlike models based on theoretical stellar atmospheres our SSP models provide good fits to the colours of the globular clusters of the Milky Way for the ages and metallicities that are derived from CMD studies. More extensive comparisons with globular cluster data and galaxies are shown in the second paper of this series (Paper II). We show the dependence of the colours as a function of age, metallicity and IMF. We find that colours involving redder filters show greater sensitivities to the IMF slope.

We also find various absorption line features and molecular bands that are very sensitive to the IMF slope throughout the whole spectral range covered by the MIUSCAT model SEDs. Among the most prominent features we find that the NaI doublet at $\sim 8200 \text{ \AA}$ increases its strength with increasing IMF slope, whereas the neighboring CaII triplet around $\sim 8600 \text{ \AA}$, decreases, confirming previous findings (e.g., Schiavon et al. 2000; Vazdekis et al. 2003; Conroy & van Dokkum 2011). Note that the NaI feature is not covered by the model SEDs based on the MILES and CaT stellar spectral libraries.

With the aid of the MIUSCAT SSP SEDs we propose a new index definition for the NaI doublet at $\sim 8200 \text{ \AA}$, NaI8200A, which has significant advantages over previous index definitions for this feature, particularly for low velocity dispersion stellar systems. NaI8200A varies with the age and the metallicity and it is particularly sensitive to the IMF slope. We propose a NaI8200A – CaT* diagram, the latter index defined in Cenarro et al. (2001), to distinguish the effects of the IMF slope if the age and the [Na/Fe] abundance are properly constrained.

Finally we show the utility of these new models for survey-oriented spectrophotometric applications. Because of the wide spectral coverage and accurate flux calibration of the MIUSCAT library stars, the SSP models are perfectly suited for being used as templates for exploiting galactic spectrophotometric data, deriving reliable estimations of ages and metallicities even for low resolution data.

The MIUSCAT model SEDs, as well as all our model predictions, can be downloaded from the miles website (<http://miles.iac.es>), where web-based facilities are available for downloading and handling these SEDs. These user-friendly tools also allow to obtain the MIUSCAT SEDs, with the corresponding line-strength indices and colours, for a variety of SFH parametrizations as well as for user-defined SFHs.

ACKNOWLEDGMENTS

We would like to thank the Indo-U.S. team for making available their stellar spectral library. We thank F. Valdes and A. Alonso for very useful clarifications on their respective libraries as well as E. Mármol-Queraltó for testing a preliminary version of the MIUSCAT SEDs that allowed us to improve the models. We also thank the referee for relevant suggestions that certainly improved the original draft. The MILES and CaT libraries were observed at the INT and JKT telescopes, respectively, on the island of La Palma, operated by the Isaac Newton Group at the Observatorio del Roque de los Muchachos of the Instituto de Astrofísica de Canarias. This research has made an extensive use of the SIMBAD data base (operated at CDS, Strasbourg, France), the NASA’s Astrophysics Data System Article Service, and the *Hipparcos* Input Catalogue. AJC and JFB acknowledges support from the Ramón y Cajal Program financed by the Spanish Ministry of Science and Innovation. AJC and JFB are *Ramón y Cajal* Fellows of the Spanish Ministry of Science and Innovation. This work has been supported by the Programa Nacional de Astronomía y Astrofísica of the Spanish Ministry of Science and Innovation under grants AYA2010-21322-C03-01 and AYA2010-21322-C03-02 and by the Generalitat Valenciana under grant PROMETEO-2009-103.

REFERENCES

- Alexander D. R., Ferguson J. W., 1994, ApJ, 437, 879
- Alloin D., Bica E., 1989, A&A, 217, 57
- Alonso A., Arribas S., Martínez-Roger C., 1995, A&A, 297, 197
- Alonso A., Arribas S., Martínez-Roger C., 1996, A&A, 313, 873
- Alonso A., Arribas S., Martínez-Roger C., 1999, A&AS, 140, 261
- An D., et al., 2009, ApJ, 700, 523
- Benítez N., et al., 2009, ApJ, 691, 241
- Bertelli G., Bressan A., Chiosi C., Fagotto F., Nasi E., 1994, A&AS, 106, 275
- Bessell M. S., Brett J. M., Wood P. R., Scholz M., 1989, A&AS, 77, 1
- Bessell M. S., Brett J. M., Scholz M., Wood P. R., 1991, A&AS, 89, 335

- Bica E., Alloin D., Schmidt A. A., 1990, *A&A*, 228, 23
- Bruzual G., Charlot S., 2003, *MNRAS*, 344, 1000
- Buser R., Kurucz R. L., 1978, *A&A*, 70, 555
- Cardiel N., Gorgas J., Cenarro J., González J.J., 1998, *A&AS*, 127, 597
- Carter D., Visvanathan N., Pickles A. J., 1986, *ApJ*, 311, 637
- Cassisi S., Castellani V., Ciarcelluti P., Piotto G., Zoccali M., 2000, *MNRAS*, 315, 679
- Cenarro A. J., Moles M., Cristóbal-Hornillos D., Gruel N., Benítez N., Marín-Franch A., 2010, *SPIE*, 7738,
- Cenarro A. J., Cardiel N., Vazdekis A., Gorgas J., 2007, *MNRAS*, 396, 1895
- Cenarro A. J., et al., 2007, *MNRAS*, 374, 664
- Cenarro A. J., Gorgas J., Vazdekis A., Cardiel N., Peletier R. F., 2003, *MNRAS*, 339, L12
- Cenarro A. J., Cardiel N., Gorgas J., Peletier R. F., Vazdekis A., Prada F., 2001, *MNRAS*, 326, 959
- Cervantes, J. L., Vazdekis A., 2009, *MNRAS*, 392, 691
- Cid Fernandes, R., Mateus, A., Sodré, L., Stasińska, G., Gomes, J. M., 2005, *MNRAS*, 358, 363
- Coelho P., Bruzual G., Charlot S., Weiss A., Barbuy B., Ferguson J. W., 2007, *MNRAS*, 382, 498
- Conroy C., Gunn J. E., 2010, *ApJ*, 712, 833
- Conroy C., van Dokkum P., 2011, arXiv:1109.0007
- Cousins A. W. J., 1980, *SAAOC*, 1, 234
- Dotter A., Chaboyer B., Jevremović D., Kostov V., Baron E., Ferguson J. W., 2008, *ApJS*, 178, 89
- Edvardsson, B., Andersen, J., Gustafsson, B., Lambert, D. L., Nissen, P. E., Tomkin, J., 1993, *A&AS*, 102, 603
- Faber S. M., French. H., 1980, *ApJ*, 235, 405
- Falcón-Barroso J., Balcells M., Peletier R., Vazdekis A., 2003, *A&A*, 405, 455
- Falcón-Barroso, J., Sánchez-Blázquez, P., Vazdekis, A., Ricciardelli, E., Cardiel, N., Cenarro, A. J., Gorgas, J., Peletier, R. F., 2011, *A&A*, 532, 95
- Fuhs M.A., Plez B., Thé P.S., de Winter D., Westerlund B.E., Steenman H.C., 1994, *A&AS*, 105, 311
- Girardi L., Bressan A., Bertelli G., Chiosi C., 2000, *A&AS*, 141, 371
- González-Delgado, R. Cerviño, M., Martins, L. P., Leitherer, C., Hauschildt, P. H., 2005, *MNRAS*, 357, 945
- Harris W. E., 1996, *AJ*, 112, 1487
- Hayes, D. S., 1985, in D. S. Hayes, L. E. Pasinetti, & A. G. D. Philip, eds. *Proc. IAU Symposium 111, Calibration of fundamental stellar quantities*. Dordrecht, Reidel, p. 225.
- Ilbert O., et al., 2009, *ApJ*, 690, 1236
- Koleva, M., Prugniel, P., Bouchard, A., & Wu, Y. 2009, *A&A*, 501, 1269
- Kroupa P., 2001, *MNRAS*, 322, 231
- Le Borgne, J.-F., Rocca-Volmerange, B., Prugniel, P., Landon, A., Fioc, M., Soubiran, C., 2004, *A&A*, 425, 881
- Lejeune T., Cuisinier, F., Buser R., 1997, *A&AS*, 125, 229
- Lejeune T., Cuisinier F., Buser R., 1998, *A&AS*, 130, 65
- Maraston C., 2005, *MNRAS*, 362, 799
- Maraston C., Strömbäck G., Thomas D., Wake D. A., Nichol R. C., 2009, *MNRAS*, 394, L107
- Maraston C., Strömbäck G., 2011, *MNRAS*, 418, 2785
- Moles M., et al., 2008, *AJ*, 136, 1325
- Peacock M. B., Zepf S. E., Maccarone T. J., Kundu A., 2011, *ApJ*, 737, 5
- Pickles A. J., 1998, *PASP*, 110, 863
- Pols O. R., Tout C. A., Eggleton P. P., Han Z., 1995, *MNRAS*, 274, 964
- Ricciardelli E., Vazdekis A., Cenarro A. J., Falcón-Barroso J., 2012, *MNRAS*, in press
- Salpeter E. E., 1955, *ApJ*, 121, 161
- Sánchez-Blázquez P., et al., 2006, *MNRAS*, 371, 703
- Santos J., F. C., Jr., Alloin D., Bica E., Bonatto C. J., 2002, *IAUS*, 207, 727
- Sarzi M., et al., 2006, *MNRAS*, 366, 1151
- Schiavon R. P., Barbuy B., Rossi S. C. F., Milone A., 1997, *ApJ*, 479, 902
- Schiavon R. P., Barbuy B., Bruzual G., 2000, *ApJ*, 532, 453
- Schiavon R. P., Caldwell N., Rose J. A., 2004, *AJ*, 127, 1513
- Schiavon R. P., 2007, *ApJS*, 171, 146
- Serven J., Worthey G., Briley M. M., 2005, *ApJ*, 627, 754
- Soubiran C., Katz D., Cayrel R., 1998, *A&AS*, 133, 221
- Tinsley, B. M., 1980, *Fundam. Cosmic Phys.*, 5, 287
- Tojeiro R., Percival W. J., Heavens A. F., Jimenez R., 2011, *MNRAS*, 413, 434
- Trager S. C., Worthey G., Faber S. M., Burstein D., González J. J., 1998, *ApJS*, 116, 1
- Valdes F., Gupta R., Rose J. A., Singh H. P., Bell D. J., 2004, *ApJS*, 152, 251
- van Dokkum P. G., Conroy C., 2010, *Nature*, 468, 940
- Vazdekis A., Sánchez-Blázquez P., Falcón-Barroso J., Cenarro A. J., Beasley M. A., Cardiel N., Gorgas J., Peletier R. F., 2010, *MNRAS*, 404, 1639
- Vazdekis A., Cenarro A. J., Gorgas J., Cardiel N., Peletier R. F., 2003, *MNRAS*, 340, 1317
- Vazdekis A., 1999, *ApJ*, 513, 224
- Vazdekis A., Arimoto N., 1999, *ApJ*, 525, 144
- Vazdekis A., Peletier R. F., Beckman J. E., Casuso E., 1997, *ApJS*, 111, 203
- Vazdekis A., Casuso E., Peletier R. F., Beckman J. E., 1996, *ApJS*, 106, 307
- Wolf C., Hildebrandt H., Taylor E. N., Meisenheimer K., 2008, *A&A*, 492, 933
- Worthey G., 1994, *ApJS*, 95, 107